Spatiotemporal Variability of Tropical Cyclone Precipitation Using a High-Resolution, Gridded (0.25° × 0.25°) Dataset for the Eastern United States, 1948–2015

JOSHUA C. BREGY

Department of Geography, and Department of Earth and Atmospheric Sciences, Indiana University, Bloomington, Indiana

JUSTIN T. MAXWELL AND SCOTT M. ROBESON

Department of Geography, Indiana University, Bloomington, Indiana

JASON T. ORTEGREN

Department of Earth and Environmental Sciences, University of West Florida, Pensacola, Florida

PETER T. SOULÉ

Department of Geography and Planning, Appalachian State University, Boone, North Carolina

PAUL A. KNAPP

Department of Geography, Environment, and Sustainability, University of North Carolina at Greensboro, Greensboro, North Carolina

(Manuscript received 2 January 2019, in final form 30 October 2019)

ABSTRACT

Tropical cyclones (TCs) are an important source of precipitation for much of the eastern United States. However, our understanding of the spatiotemporal variability of tropical cyclone precipitation (TCP) and the connections to large-scale atmospheric circulation is limited by irregularly distributed rain gauges and short records of satellite measurements. To address this, we developed a new gridded (0.25° × 0.25°) publicly available dataset of TCP (1948–2015; Tropical Cyclone Precipitation Dataset, or TCPDat) using TC tracks to identify TCP within an existing gridded precipitation dataset. TCPDat was used to characterize total June–November TCP and percentage contribution to total June–November precipitation. TCP totals and contributions had maxima on the Louisiana, North Carolina, and Texas coasts, substantially decreasing farther inland at rates of approximately 6.2–6.7 mm km^{-1}. Few statistically significant trends were discovered in either TCP totals or percentage contribution. TCP is positively related to an index of the position and strength of the western flank of the North Atlantic subtropical high (NASH), with the strongest correlations concentrated in the southeastern United States. Weaker inverse correlations between TCP and El Niño–Southern Oscillation are seen throughout the study site. Ultimately, spatial variations of TCP are more closely linked to variations in the NASH flank position or strength than to the ENSO index. The TCP dataset developed in this study is an important step in understanding hurricane–climate interactions and the impacts of TCs on communities, water resources, and ecosystems in the eastern United States.

Supplemental information related to this paper is available at the Journals Online website: https://doi.org/10.1175/JCLI-D-18-0885.s1.

Corresponding author: Joshua C. Bregy, jbregy@indiana.edu

DOI: 10.1175/JCLI-D-18-0885.1

1. Introduction

Tropical cyclone precipitation (TCP) is an important part of the hydroclimate in the southeastern United States (Knight and Davis 2007). However, inland flooding from excessive TCP is a widespread natural hazard. One notable example of TCP-induced flooding is Hurricane Harvey (2017), which produced record-breaking rainfall that exceeded 1500 mm in some locations in Texas (Risser and Wehner 2017; Trenberth et al. 2018; Zhang et al. 2018). In addition to flooding, excessive rainfall from tropical cyclones (TCs) can trigger other hazards including mass wasting along saturated slopes (e.g., Lin et al. 2008; Wooten et al. 2008; Antinao and Farfán 2013; Kuo et al. 2013; Cogan et al. 2018; Yanites et al. 2018), outbreaks of infectious diseases (e.g., Lin et al. 2012; Kim et al. 2013; Deng et al. 2015; Fredrick et al. 2015; Zheng et al. 2017), and infrastructure damage and failure (Guiney 2007; Czajkowski et al. 2013; Mondoro and Frangopol 2018; Yang et al. 2019). While excess TCP is hazardous, TCP is also an important contributor to annual water budgets in the region (Cry 1967; Knight and Davis 2007; Nogueira and Keim 2011), can expedite drought cessation (Maxwell et al. 2012, 2013, 2017; Kam et al. 2014; Brun and Barros 2014), and can be an important abiotic control on biodiversity and ecosystem structure (Walls et al. 2013; Chi et al. 2015; Goulding et al. 2016; Knapp et al. 2016). The dichotomous nature of TCP underlines the importance of understanding TCP variability and determining connections to large-scale atmospheric variability to elucidate spatiotemporal patterns in TCP–climate interactions.

Numerous studies have examined individual storms or TCs over smaller spatial scales to understand the atmospheric circulation patterns and ambient conditions (e.g., sea surface temperatures) giving rise to anomalous amounts of TCP (e.g., Zhu and Zhang 2006; Konrad and Perry 2010; Chien and Kuo 2011; Hall et al. 2013; Hernández Ayala and Matyas 2016; Matyas 2017; Trenberth et al. 2018). Relatively few studies have examined TCP from the context of regional or global hydroclimates. Cry (1967) provided one of the earliest TCP climatologies (1931–60) for the East Coast of the United States using surface observations from locations frequently impacted by TCs. Building on the work of Cry (1967), Knight and Davis (2007) developed a TCP climatology (1980–2004) in the mid-Atlantic and southeastern United States using first-order surface observations and the Cooperative Observer Program (COOP). However, they did not distinguish between TCP and extratropical precipitation (Knight and Davis 2007), making the two studies difficult to compare. Importantly, Knight and Davis (2009) found that the frequency of TCP events and their contribution to extreme precipitation events in the southeastern United States were increasing. Nogueira and Keim (2011) show broadly similar spatial patterns in the eastern United States, with the greatest annual average TCP located in south Florida (120–130 cm), while additional areas of high values (90–120 cm) occur in central/north Florida, southeast North Carolina, and the northern Gulf Coast. Generally, their estimates of TCP contributions to seasonal precipitation were similar to the results in Cry (1967). However, contributions of TCP to seasonal precipitation farther inland were greater than previous estimates (Cry 1967) by ~2% yr^{-1}, which Nogueira and Keim (2011) attribute to a different study period (1960–2007) and greater station density. The difference between studies becomes more apparent in the mean monthly TCP contribution; Nogueira and Keim (2011) report TCP contributions that are approximately half of the values shown in previous work (Knight and Davis 2007). In addition to the aforementioned factors, selection criteria (e.g., inclusion/exclusion of extratropical cyclones) and storm track density may explain differences in mean monthly TCP contributions between studies (Nogueira and Keim 2011).

While gauge-based studies have helped to understand historical TCP variability, missing observations and the irregular distribution of rain gauges limit interpretability. Efforts to address this problem often employ satellite or radar measurements of TCP (e.g., Rodgers et al. 1994; Rodgers and Pierce 1995; Rodgers et al. 2001; Lonfat et al. 2004; Benedetti et al. 2005; Shepherd et al. 2007; Jiang and Zipser 2010; Jiang and Ramirez 2013; Prat and Nelson 2013a,b; Zhu and Quiring 2017; Rios Gaona et al. 2018; Tang and Matyas 2018). Using satellite measurements improves data coverage. For example, the Tropical Rainfall Measuring Mission (TRMM) Multisatellite Precipitation Analysis 3B42 and 3B43 provide subdaily measurements from 50°N to 50°S at a resolution of 0.25°. These improvements have prompted multiple studies examining recent changes in TCP within and beyond the spatial coverage provided by most stations (e.g., Lonfat et al. 2004; Jiang and Zipser 2010; Prat and Nelson 2013a,b; Xu et al. 2014; Zick and Matyas 2015; Zhu and Quiring 2017). However, satellite-based TCP climatologies are currently limited by a short record length (e.g., Defense Meteorological Satellite Program Special Sensor Microwave Imager: 1987–present; TRMM: 1997–2015; Global Precipitation Measurement: 2014–present), making them less useful for assessing TCP interactions with low-frequency climate oscillations (Ashouri et al. 2015; Zhu and Quiring 2017).

The influence of El Niño–Southern Oscillation (ENSO) on tropical cyclone activity for the North Atlantic is well documented, with the warm (El Niño)

and cool (La Niña) phases associated with decreased and increased TC frequency, respectively (e.g., Gray 1984; Bove et al. 1998; Elsner et al. 2001; Smith et al. 2007). The few studies that have examined the relationship between TCP and large-scale atmospheric–oceanic variability focus on ENSO, the Atlantic multidecadal oscillation, or the North Atlantic Oscillation (Nogueira et al. 2013; Khouakhi et al. 2017; Aryal et al. 2018), but no studies have examined the connection between TCP patterns and the North Atlantic subtropical high. Nogueira et al. (2013) found that ENSO was driving increased spatial variability in TCP for certain regions of the eastern United States, particularly in Texas. This pattern is attributed to the change in landfall frequency in response to shifts in ENSO phases (Nogueira et al. 2013). Likewise, Khouakhi et al. (2017) demonstrated that La Niña is generally responsible for the increased extreme precipitation arising from TCs. They suggest that what underlies the control ENSO has on TCP is the fact that there is a heightened probability of TCs impacting the United States simply due to the increased number of storms generated during La Niña.

Relative to ENSO, less attention has been focused on the role of the North Atlantic subtropical high (NASH; often referred to as the Azores or Bermuda high) on TCP. Instead, studies often use the North Atlantic Oscillation (NAO) to represent atmospheric circulation patterns in the North Atlantic (e.g., Elsner et al. 2000, 2001; Aryal et al. 2018). However, the NAO is considered to be the dominant mode of circulation only during the winter. The NASH is a semipermanent anticyclone that migrates between Bermuda and the Azores (Sahsamanoglou 1990; Davis et al. 1997). It is the dominant form of circulation during summer and fall (Davis et al. 1997); consequently, it can directly influence summer precipitation in the southeastern United States (Li et al. 2011, 2012). Several studies suggest that shifts in the position, size, or intensity of the NASH have a strong influence on TC tracks (Liu and Fearn 2000; Elsner et al. 2000, 2001; Glaser et al. 2013), which can impact spatiotemporal patterns of TCP.

To overcome the limitations of gauge- and satellite-based analyses, we developed a long-term, high-resolution, gridded dataset of TCP that is publicly available (see section 4). Using an existing gridded (0.25° × 0.25°) precipitation dataset, we extracted TCP for the eastern United States by integrating TC track information on a subdaily basis. We used this newly developed Tropical Cyclone Precipitation Dataset (TCPDat) to 1) examine the spatial patterns of TCP and the contribution of TCP to seasonal rainfall for the eastern United States, 2) test for trends in TCP, and 3) identify the role of large-scale atmospheric–oceanic variability on TCP patterns.

2. Materials and methods

a. Tropical cyclones

To determine the position and intensity of TCs, we used the tropical cyclone best track data from the Hurricane Database (HURDAT2) (Landsea et al. 2004; Landsea and Franklin 2013), available from the World Meteorological Organization's International Best Track Archive for Climate Stewardship initiative v03r09 (Knapp et al. 2010). The regularly updated database includes best track data from the season preceding the current Atlantic hurricane season and extends to 1851. The accuracy and completeness of the dataset prior to aircraft reconnaissance (pre-1944) and satellite monitoring (pre-1972) is limited because of uncertainties in the best track parameters (e.g., position, intensity, wind radii; Hagen et al. 2012; Torn and Snyder 2012; Landsea and Franklin 2013; Landsea et al. 2014) used in the reanalysis. The precipitation data that we used, and consequently our study period, begin in 1948, so we also avoided many of the problems that come with using pre-1944 reanalyses (Vecchi and Knutson 2011). While a portion of our study period lacked satellite observations (1948–71), tropical cyclones that impacted the eastern conterminous United States (CONUS) were well observed by in situ data sources during this period.

We defined a TC as a tropical depression, tropical storm, or hurricane. Following this definition, storms that were entirely extratropical or subtropical were removed from the dataset. We also excluded any portions of the life cycle of a given TC during which it was in the subtropical or extratropical phase. Likewise, we excluded any nontropical precursor classification. In all cases, we used the system status (e.g., tropical depression [TD], hurricane [HU], extratropical cyclone [EX], subtropical storm [SS]) from HURDAT2 to identify and remove nontropical cyclones and nontropical stages. Given that the initiation of storm transition is not identified in HURDAT2, our selection criteria for a TC include the transition period during which storms are a hybrid between tropical and nontropical cyclones. While transitioning storms have both tropical and nontropical characteristics (Evans and Hart 2003; Hart et al. 2006), we assume that the system status indicated by HURDAT2 is the most accurate characterization of the storm. We further refined the dataset by removing any storms that were not within 223 km of any landmass, in accordance with the average precipitation radius of a TC (Matyas 2010). This radius allowed us to capture TCP over the CONUS for nearshore TCs that never made landfall. Finally, HURDAT2 storm entries are recorded at 6-h intervals. Consequently, fast-moving TCs can move large distances between entries. To address this,

we used a cubic spline to spatially interpolate TC position (i.e., eye coordinates) between observations, doubling the number of position entries per TC.

b. Precipitation

We used daily precipitation data from the Climate Prediction Center (CPC) U.S. Unified Precipitation (URD) dataset (Higgins et al. 2000a) provided by NOAA/OAR/ESRL Physical Sciences Division. A comprehensive discussion about the development of the CPC gridded precipitation dataset can be found in Higgins et al. (2000b). URD is updated daily (−1200 to 1200 UTC) to provide high-resolution (0.25° × 0.25°) gridded precipitation over the CONUS since 1948 (Higgins et al. 2000b, 2008). Precipitation data from more than 8000 stations in the CPC unified rain gauge dataset are interpolated to a grid using an optimal interpolation (OI; Gandin 1965) scheme (Chen et al. 2008; Higgins et al. 2008; Higgins and Kousky 2013). Grid points are built using the weighted mean of observed and first-guess value differences among stations within the specified search distance (Gandin 1965; Chen et al. 2008). The weighted coefficient used in OI is determined using the precipitation field variance and covariance structures (Gandin 1965; Chen et al. 2008). This is unique because unlike the Cressman and Shepard techniques (Cressman 1959; Shepard 1968), OI does not solely rely on the distance between grid points and station gauges to determine the weighted coefficient (Gandin 1965; Chen et al. 2008). Rather, OI constructs fields of daily precipitation climatologies based on historical station observations (Xie et al. 2007; Chen et al. 2008). The resulting gridded fields consist of interpolated ratios between the daily precipitation and daily climatologies, which are then multiplied by the daily climatology to yield daily precipitation analyses (Xie et al. 2007; Chen et al. 2008). Interpolating with the ratio makes the OI technique especially powerful for characterizing the spatial patterns of precipitation (Chen et al. 2008). Moreover, analysis of different interpolation techniques indicates that OI consistently outperforms other techniques when applied to daily precipitation analysis and representing spatial patterns of precipitation (Chen et al. 2008).

URD is widely used in hydroclimatological studies as it is perhaps the most spatiotemporally complete daily precipitation dataset covering the CONUS (Atallah et al. 2007; Corbosiero et al. 2009; Higgins and Kousky 2013; Aryal et al. 2018; Luitel et al. 2018). While individual intense precipitation events are often not accurately represented by URD due to smoothing, the differences between gauge-based and URD-based seasonal and annual rainfall totals are small (Atallah et al. 2007; Ensor and Robeson 2008). Presumably, the similarities between gauge- and URD-based seasonal and annual totals persist over longer (e.g., decadal or multidecadal) intervals. Ultimately, while smoothing is an issue with URD, which can limit its utility in certain applications where gauge-based data are preferred (e.g., recurrence intervals; Ensor and Robeson 2008), the lack of missing data and the gridded structure of URD are strengths that result in a spatiotemporally complete dataset.

URD has been successfully applied to the eastern Pacific to understand the TC hydroclimate of the southwest United States (Corbosiero et al. 2009). Despite ~10% of Pacific TCs occurring in the eastern Pacific, URD has shown that these TCs are an important water source for regional hydroclimates, contributing between 5% and 20% of annual precipitation throughout the southwestern United States (Corbosiero et al. 2009). Further, the results presented by Corbosiero et al. (2009) demonstrate that the use of gridded data such as URD can yield a robust climatology of TCP, in spite of the difficulty URD has with capturing mesoscale phenomena (Atallah et al. 2007; Archambault et al. 2008; Ensor and Robeson 2008). We focused on TCP during the North Atlantic hurricane season, from 1 June to 30 November (JJASON), used in many North Atlantic TCP studies (e.g., Knight and Davis 2007, 2009; Nogueira and Keim 2010; Zhou and Matyas 2017) as seasonal TCP values should largely reflect annual TCP values. Hence, values for total TCP and its contribution to total rainfall represent JJASON rather than an entire year.

c. Tropical cyclone precipitation extraction

To extract TCP from the precipitation dataset, we identified all grid points within a 223-km radius (Matyas 2010) from the interpolated TC position. Although the shape of the TC rain field changes after landfall and cannot be fully captured with a circle (Matyas 2007, 2013; Villarini et al. 2011), we used the average size of a TC rain field (223 km; Matyas 2010) to construct a search radius, reducing the probability that nontropical precipitation is captured in TCPDat. Other approaches have been employed by examining TCP over multiple radii (e.g., Konrad et al. 2002) as well as using a liberal search radius (e.g., 500 km; Nogueira and Keim 2011). While these approaches have yielded invaluable information on the TCP hydroclimate, we elected to use a more conservative radius (223 km) to examine variable minima in extreme precipitation.

Using subdaily interpolated TC tracks risks precipitation at a given grid cell being counted multiple times. To account for this, we built a gridded Boolean presence–absence matrix for each daily precipitation

period. At each grid point, we then calculated multiple metrics, including total JJASON TCP, monthly total TCP, mean JJASON TCP, and JJASON TCP contribution to total seasonal precipitation. We performed a monotonic trend analysis on the total sum of JJASON TCP and the JJASON TCP contribution using the nonparametric Mann–Kendall test, which is widely used in climate studies for its resistance to outliers (e.g., Tabari et al. 2011; Gocic and Trajkovic 2013; Ficklin et al. 2015; Maxwell et al. 2017; Aryal et al. 2018). Setting the significance threshold at $\alpha = 0.05$, we used the Mann–Kendall z scores to identify locations with increasing ($z > 0$) and decreasing ($z < 0$) TCP. Before trend analysis, we tested for autocorrelation and found that TCP values were not autocorrelated.

d. Climate indices

To examine the role of large-scale atmospheric circulation and climate modes on TCP, we targeted climate indices known to influence TC genesis, development, and/or tracks. Specifically, we selected mean monthly index values representative of the NASH and ENSO. While the Atlantic multidecadal oscillation is thought to influence TCs (Klotzbach and Gray 2008; Wang et al. 2008; Enfield and Cid-Serrano 2010), there are only a limited number of complete cycles over our period of record, and therefore we elected to focus on indices with important roles on interannual TC variability. Despite the influence of the NAO on TCs (Elsner and Kocher 2000; McCloskey et al. 2013), the NASH is a direct representation of atmospheric circulation in the region of the North Atlantic where TCs develop and track (McCloskey et al. 2013). While the central core of the NASH is usually positioned in the central or eastern Atlantic, the center of circulation typically moves west during summer, positioning the western edge of the NASH over the southeastern United States. Summer precipitation patterns may shift in response to this motion (Stahle and Cleaveland 1992; Davis et al. 1997; Katz et al. 2003; Li et al. 2011; Li et al. 2012). The magnitude of western migration often is quantified using the Bermuda high index (BHI), which represents the normalized sea level pressure gradient between New Orleans (Louisiana) and Bermuda (Stahle and Cleaveland 1992; Katz et al. 2003; Ortegren et al. 2011). Negative (positive) values indicate that the western flank of the NASH is positioned farther west (east) closer to New Orleans (Bermuda) (Ortegren and Maxwell 2014). The BHI does not provide information regarding the position of the NASH or its strength; rather, it explicitly defines meridional variations in the western ridge of the anticyclone. Furthermore, it does not entirely capture zonal variations in western flank position (Ortegren and Maxwell 2014), which can be an important control on precipitation variability in the southeastern United States (Li et al. 2011, 2012). We also retrieved index values for the NAO index for September–October from Li and Wang (2003). This index extends back to 1948 and represents the standardized pressure gradient between the Azores and Iceland. Finally, we used the bivariate ENSO time series (BEST; Smith and Sardeshmukh 2000) index (1948–2015; 3-month moving average) from NOAA/OAR/ESRL PSD. We selected the BEST dataset as it fully represents oceanic and atmospheric processes by combining the Niño-3.4 SST index with the Southern Oscillation index (SOI).

To identify potential relationships between the large-scale forcings of TCP, we conducted a spatial field correlation between the gridded TCP metrics and the climate indices using Kendall's tau-b. To examine the combined effect of ENSO and BHI, we used both indices as predictors in a linear regression model against logged TCP. To account for the multiple zeros, we added 1 mm to every year of TCP prior to taking the natural log of TCP. Finally, we used empirical orthogonal function (EOF) analysis to identify spatial patterns associated with the primary modes of variability. Using the seasonal total TCP and TCP contribution, EOF analysis produced eigenvectors, principal component (PC) time series, and eigenvalues that we used to identify primary modes of variability and potential climate connections. We tested whether the first five PC time series (which indicate the amplitudes of the leading modes of variability) were correlated with the contemporaneous ENSO and BHI values using Spearman's rank correlation. The color schema of our maps were created using "cmocean mfiles" (Thyng et al. 2016).

3. Results and discussion

a. Total JJASON TCP and TCP contributions to total JJASON precipitation

Our TCP and TCP contribution results show the expected major features presented in previous studies (Knight and Davis 2007; Nogueira and Keim 2011), but with gridded data at high spatial resolution over a long period of time (Figs. 1 and 2). The highest values of mean JJASON TCP (Fig. 1) and mean JJASON TCP contribution (Fig. 2) are concentrated along the Gulf and Southeast Coasts, which have the greatest number of years with at least one TC (≥40 years; see Fig. S1 in the online supplemental material). Generally, our mean TCP (Fig. 1) and mean TCP contributions (Fig. 2) are lower than previous studies (e.g., Knight and Davis 2007;

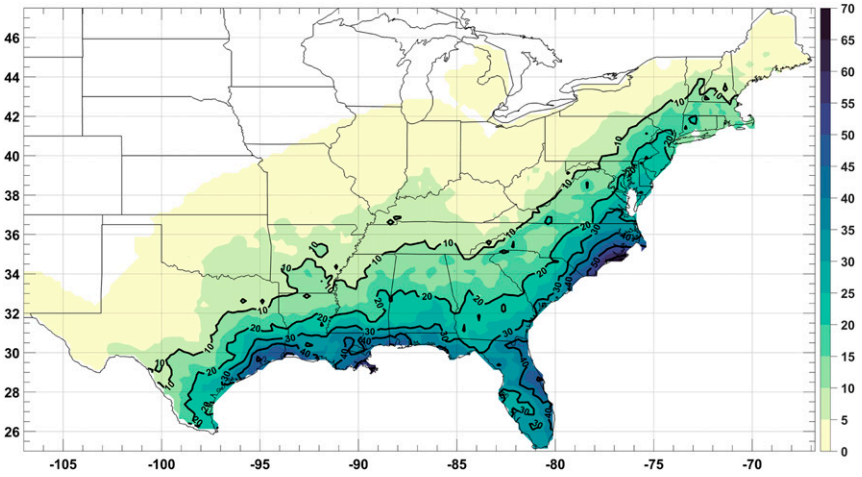

FIG. 1. Map of the mean seasonal (JJASON) TCP (mm yr^{-1}) during 1948–2015 for 0.25° × 0.25° grid.

Nogueira and Keim 2011), sometimes by approximately 50% in areas with higher contributions.

Our results differ slightly from previous studies (Knight and Davis 2007; Nogueira and Keim 2011) likely because of data and methodological differences, including different search radii and the inclusion or exclusion of extratropical precipitation. At 68 years (1948–2015), our study period was the longest. The increase in record length alone provides more reliable estimates of TCP patterns. Another possible explanation is the difference between gridded and point data (Ensor and Robeson 2008). Two studies used precipitation data from either the United States Historical Climatology Network (USHCN; Nogueira and Keim 2011) or first-order station datasets/COOP (Knight and Davis 2007). While these approaches use reliable data, TCP patterns are not fully represented due to nonuniform station coverage. Although our precipitation dataset relies on station data (Higgins et al. 2000a), an interpolation scheme is applied beforehand (Higgins et al. 2007; Xie et al. 2007; Higgins and Kousky 2013), producing a high-resolution dataset with no missing values. As such, the use of a gridded dataset could produce slightly different results from those seen in point-based data (Ensor and Robeson 2008). Finally, extraction techniques can affect TCP patterns by over- or underestimating TCP (Hewitson and Crane 2005; Ensor and Robeson 2008), particularly if precipitation from extratropical cyclones or frontal systems is included. Knight and Davis (2007) included precipitation from extratropical cyclones and

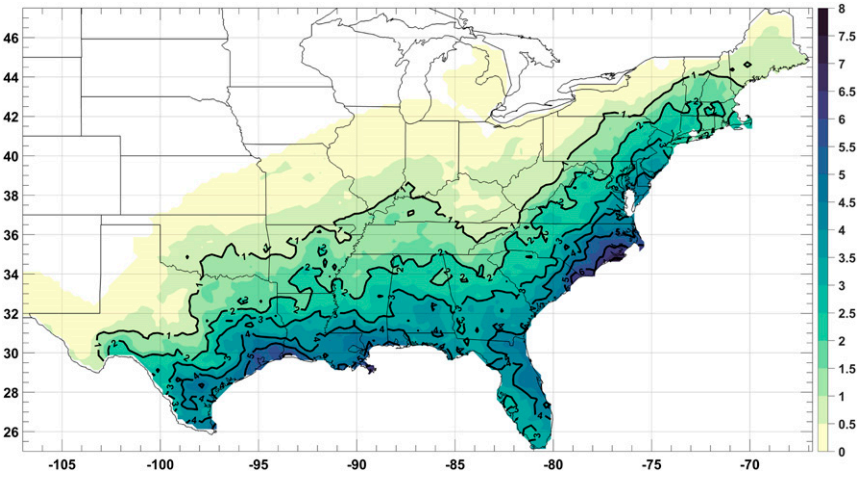

FIG. 2. Map of the mean seasonal (JJASON) contribution (% yr^{-1}) of TCP to seasonal precipitation during 1948–2015 for 0.25° × 0.25° grid.

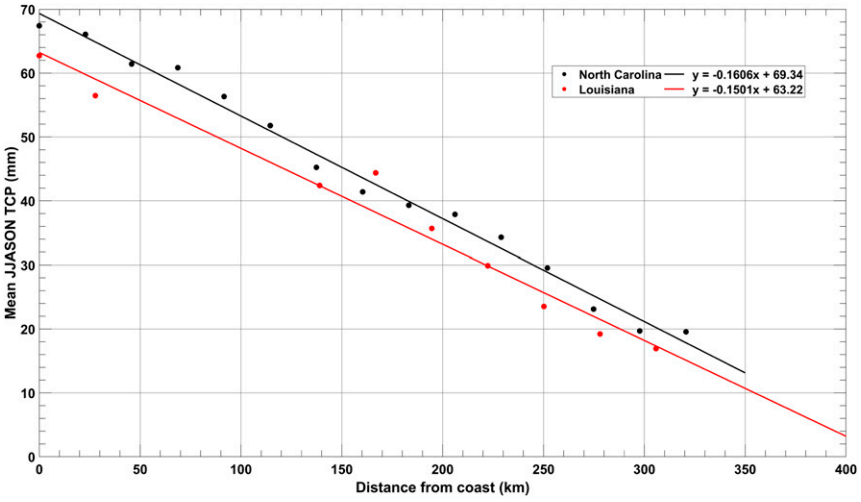

FIG. 3. Spatial gradients for mean JJASON TCP from the coast to ~300 km inland along a constant parallel for North Carolina (black; starting coordinates: 34.9°N, 76.3°W; $R^2 = 0.9895$) and a constant meridian for Louisiana (red; starting coordinates: 29.3°N, 89.4°W; $R^2 = 0.9721$). TCP beyond ~300 km inland plateaus (not shown).

potentially frontal (nontropical) systems in their analysis. Nogueira and Keim (2011) avoided collecting extratropical precipitation by only including storms given a ''tropical'' rating in HURDAT. However, considering the extreme changes in TCP distribution that occur postlandfall (Atallah et al. 2007; Matyas 2007, 2010), the larger 500-km search radius used by Nogueira and Keim (2010, 2011) to extract TCP could have included frontal and other nontropical precipitation. While our selection of a 223-km radius (Matyas 2010) could lead us to underestimate actual TCP, it increases the probability that the extracted precipitation arises primarily from TCs rather than non-tropical-cyclogenic sources.

To determine whether the difference between previous studies and this one was related to the conservative search radius, we analyzed mean TCP and mean TCP contributions using a similar search radius (500 km) and study period (1960–2007) as Nogueira and Keim (2011). Mean TCP from TCPDat was consistently less than previous studies (Figs. S2 and S3). The spatial patterns predominantly match our results using a 223-km radius (Fig. 1), such as maxima located along much of the Gulf Coast, Florida, and North Carolina. TCP contribution also increased substantially (Figs. S4 and S5) and were closer to the values presented by Nogueira and Keim (2011) and Knight and Davis (2007). Additionally, there was no difference in TCP contribution between the two different study periods using TCPDat (i.e., 1948–2015 and 1960–2007; Figs. S4 and S5). The spatial patterns of TCP contributions using a 500-km radius (Figs. S4 and S5) and a 223-km radius (Fig. 2) were virtually identical. Furthermore, our analysis of rainfall from Hurricane Georges (Figs. S6, S7) using two different radii, 223 and 500 km, reveals that TCPDat generally mirrors the spatial patterns of maps of poststorm precipitation analysis from NHC—particularly with the 500-km radius—while underestimating the most extreme rainfall values during individual events. Differences between the two radii largely stem from storm characteristics (e.g., storm size), indicating that storm-specific radii are required to analyze individual events. In either case, this is consistent with results from previous studies showing that individual extreme events are not well represented by URD on subseasonal to event-based time scales (Ensor and Robeson 2008). Despite its underperformance in this capacity, TCPDat still provides an accurate representation of TCP climatology over longer time scales. Our results (Figs. 1 and 2; see also Figs. S2–S7) support the notion that the differences between this study and previous TCP climatologies arise from our use of gridded data from URD, and that TCPDat provides an accurate estimation of the TC hydroclimate in the eastern United States.

We calculated the gradient in mean JJASON TCP (Fig. 3) from the coast to ~300 km inland to further illustrate the utility of TCPDat in examining varying TCP spatial patterns. Mean JJASON TCP contribution was calculated but not shown because of its similarity to mean JJASON TCP (Fig. 3). The TCP gradient for North Carolina [16.06 mm $(100\,\text{km})^{-1}$; $r^2 = 0.9895$] decreases more rapidly than the gradient in Louisiana [15.01 mm $(100\,\text{km})^{-1}$; $r^2 = 0.9721$; Fig. 3]. Similar to previous studies (e.g., Khouakhi et al. 2017), both transects show that decreases in mean JJASON TCP remains linear for approximately 300 km inland before

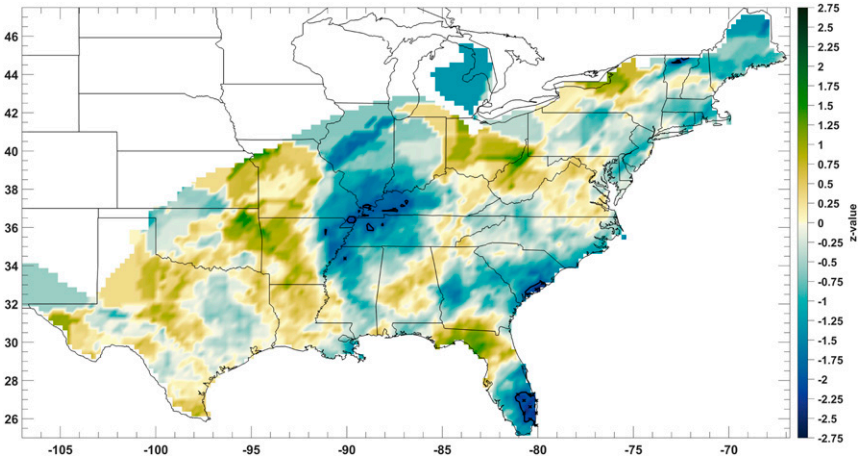

FIG. 4. Mann–Kendall trend for seasonal JJASON TCP from 1948 to 2015. Contours and hatching indicate regions of significance ($p \leq 0.05$).

transitioning to a plateau in TCP (not shown). While we do not examine some of the more nuanced changes possibly due to topographic interactions (e.g., Schwarz 1970; Harville 2009; Rostom and Lin 2015) or changes in storm tracks (Rostom and Lin 2015; Liu et al. 2016), the gridded nature of TCPDat allows for the examination of spatial changes in TCP without requiring substantial interpolation.

b. *Trends in TCP*

Our results do not show the same patterns in trends in TCP as seen in previous studies (Knight and Davis 2007; Nogueira et al. 2013). Except for small, isolated locations (i.e., negative trends in Florida and the Mississippi River Valley), we did not find any trends in total JJASON TCP (Fig. 4) or JJASON percentage contribution, which is not shown as it similar to Fig. 4. A more varied pattern was reported by Nogueira et al. (2013), where increasing (decreasing) TCP occurs at 75% (25%) of stations with significant trends. Most stations along the Gulf Coast indicate increasing TCP, while trends along the East Coast are more varied (Nogueira et al. 2013). South Florida is the only area showing a significant trend in our results (Fig. 3) that spatially overlaps with stations in Knight and Davis (2007) and Nogueira et al. (2013), but our analysis indicates that the trend there is negative, in contrast to previous findings.

c. *TCP and climate: NASH*

We found limited significant relationships between interannual TCP variations and the NAO index (Li and Wang 2003), with the summer (JJA) season showing no significant correlations (not shown) and fall (SON) season having spatially limited significance (Fig. 5). Significant correlations are primarily located on the edges of TCPDat (Fig. 5). While the NAO index may exhibit an influence on TCP along the coast, the significant correlations observed well inland are likely spurious. Moreover, although the correlations between TCP and the NAO Index along the coast are spatially limited (Fig. 5), they occupy the same area as correlations between TCP and the index used for the NASH (Fig. 6). Given that the NAO is calculated from the pressure gradient between the Azores Islands and the Icelandic low, and therefore indicates the midlatitude pressure gradient of which the NASH is one component, we focus on the NASH as it is the physical feature closer to the main development region (Davis et al. 1997) and has a strong influence on the overall hydroclimate of the southeastern United States (Li et al. 2011, 2012; Ortegren and Maxwell 2014).

The correlation analyses between the Bermuda high index (BHI; Ortegren et al. 2011) and different TCP metrics indicate a number of significant relationships. Positive correlations between TCP and BHI are seen throughout the eastern United States, with the exception of the north-central/northwestern Midwest, New England, and isolated locations in the southern Great Plains and coastal Southeast (Fig. 6). A large spatially continuous region of the eastern United States shows a significant ($p \leq 0.05$) positive correlation ($0.2 \leq r < 0.5$) between the two variables, with the strongest correlations ($0.4 \leq r < 0.5$) present in a portion of the U.S. Southeast and the southern Appalachian highlands. The strong correlation present along the southern Appalachian Mountains may stem from precipitation intensification due to orographic lift. However, this could ultimately be a consequence of the NASH steering TCs (e.g., Vega and Binkley 1993; Elsner et al. 2000; Colbert and Soden 2012). Another smaller region of

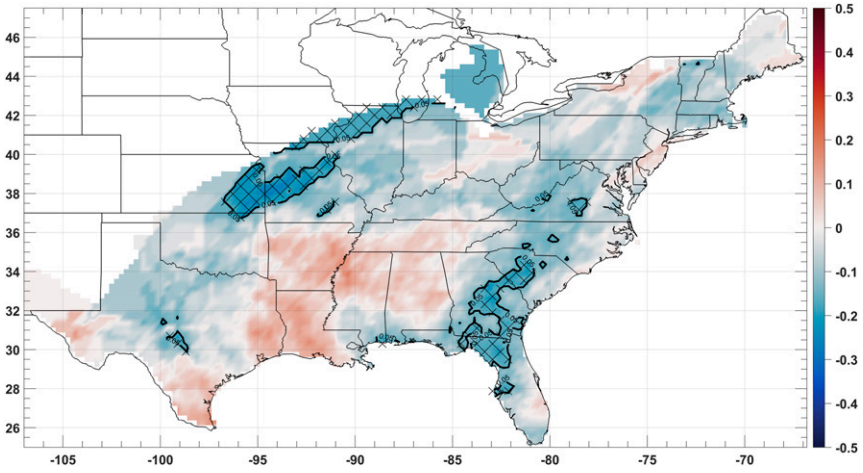

FIG. 5. Correlation analysis (Kendall's tau-b) between time series of seasonal total TCP and the NAO index for September–November. Contours and hatching indicate regions of significance ($p \leq 0.05$).

significance is present in south-central Florida, where there is also a weak positive correlation between TCP and BHI ($0.1 \leq r \leq 0.2$). Overall, this relationship suggests that during periods when the western flank of the NASH is displaced west of its mean location (i.e., BHI becomes negative), TCP tends to be suppressed relative to the mean. Conversely, when the western ridge of the NASH is displaced eastward, TCP in our study area tends to be greater than average. TCP contribution (not shown) exhibits a virtually identical magnitude and pattern as total seasonal TCP (Fig. 6).

Changes in NASH position and/or strength are frequently identified as a control on TC track variability in the North Atlantic (e.g., Vega and Binkley 1993; Elsner et al. 2000; Colbert and Soden 2012). The NASH can either act as a blocking or steering mechanism for TCs, directing storms into different regions of the North Atlantic (Vega and Binkley 1993; Elsner et al. 2000; Colbert and Soden 2012). The position and/or strength of the NASH yields environments conducive to particular TC tracks (Colbert and Soden 2012). When the anticyclone moves east and is weak, TCs tend to recurve out to sea without impacting the eastern United States (Colbert and Soden 2012). Conversely, TCs tend to either take a straight-line track or recurve before landfall when the NASH is farther west and the sea level pressure gradient (SLP) is stronger (Colbert and Soden 2012). To our knowledge, no study has explicitly examined the relationship between the NASH and TCP. The findings of the influence of the NASH—especially

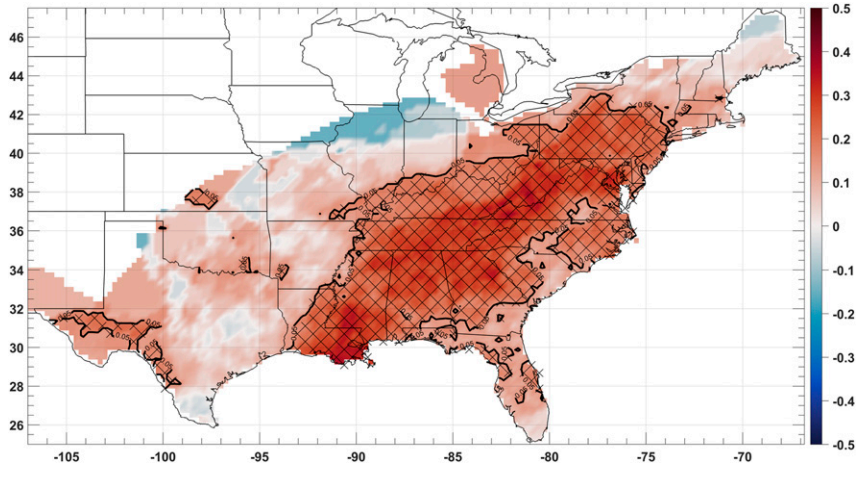

FIG. 6. Correlation analysis (Kendall's tau-b) between time series of seasonal total TCP and mean JJASON BHI. Contours and hatching indicate regions of significance ($p \leq 0.05$).

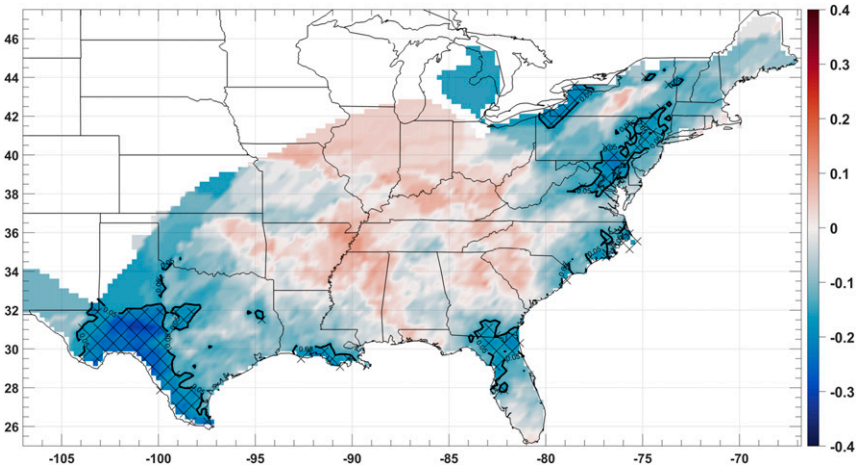

FIG. 7. Correlation analysis (Kendall's tau-b) between time series of seasonal total TCP and mean JJASON ENSO–BEST values. Contours and hatching indicate regions of significance ($p \leq 0.05$).

the western flank—on increasing variability in summertime precipitation (Li et al. 2011, 2012) demonstrate the importance of the NASH on the precipitation in the Southeast. We find that the western flank of the NASH has a significant influence on TCP, and that this could contribute to the increased variability of hurricane season rainfall. However, as the BHI does not capture zonal patterns of western flank position (Ortegren and Maxwell 2014), which adds another dimension of precipitation variability in the Southeast United States (Li et al. 2011, 2012), the relationship is likely more nuanced than what we describe above.

d. TCP and climate: ENSO

The relationship between ENSO and North Atlantic TCs is well documented (e.g., Gray 1984; Bove et al. 1998; Elsner et al. 2001; Smith et al. 2007; Yang et al. 2018). During the warm phase (El Niño), TC frequency decreases in the North Atlantic primarily due to increased vertical wind shear (e.g., Gray 1984; Bove et al. 1998). Conversely, the cool phase (La Niña) weakens vertical wind shear and produces a typically more favorable environment for tropical cyclogenesis in the region (e.g., Gray 1984; Bove et al. 1998). Although multiple studies have investigated the relationship between ENSO and TC activity, relatively few studies have examined the influence of ENSO on TCP patterns in the United States (e.g., Nogueira and Keim 2010, 2011; Nogueira et al. 2013; Khouakhi et al. 2017; Aryal et al. 2018). Given the documented inverse relationship between ENSO and TC activity (e.g., Gray 1984; Bove et al. 1998; Elsner et al. 2001; Smith et al. 2007), we expect TCP to respond similarly to ENSO.

The eastern United States displays some spatially heterogeneous patterns between total seasonal TCP and mean JJASON ENSO–BEST (Fig. 7). Much of the study area is characterized by an insignificant relationship ($-0.2 \leq r \leq 0.2$) between TCP and ENSO, which are generally grouped together with the exception of isolated corridors of opposing correlations (e.g., positive r values in upstate New York surrounded by negative r values; Fig. 7). The lack of significance across much of the eastern United States is not surprising as TCs often have already undergone extratropical transition when well inland (Hart and Evans 2001). There are isolated areas of weak to moderate significant inverse correlations ($-0.4 \leq r < 0$) between TCP and ENSO throughout the eastern United States (Fig. 7), with the most pronounced inverse relationship ($-0.4 \leq r \leq -0.3$) located in west-central Texas. In addition to the increased spatial heterogeneity in correlations compared to the NASH, a smaller portion of the study area exhibits a significant relationship ($p \leq 0.05$). The North Carolina coastal plain, northern Mid-Atlantic, northern Florida, and west-central Texas exhibit an inverse relationship ($-0.4 < r \leq -0.2$) between TCP and ENSO. Although the cool phase of ENSO is associated with increased TC frequency (e.g., Gray 1984; Bove et al. 1998), we find that TCP has a weak to moderate relationship with ENSO. The correlation between TCP contribution and ENSO (not shown) is virtually identical to total seasonal TCP in both magnitude and spatial distribution.

e. Leading mode of variability

The correlation analyses discussed in previous sections are ideal for characterizing individual relationships

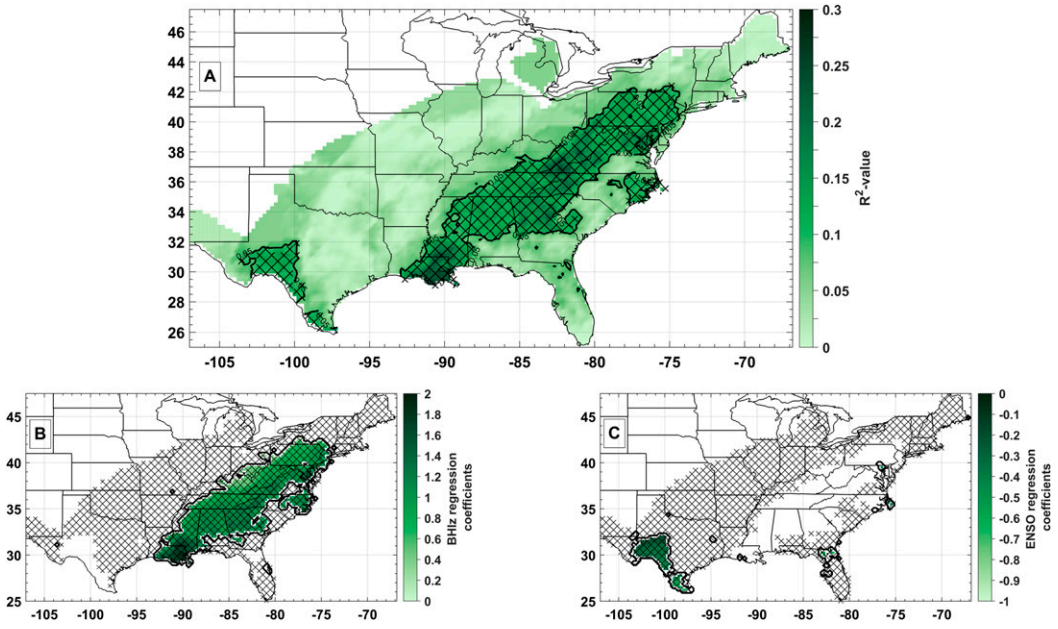

FIG. 8. (a) R^2 and (b),(c) regression coefficients for regression model incorporating BHI and ENSO, respectively. Contours represent the areas of significance ($p < 0.05$). In (a) the hatching represents significant R^2 values. In (b) the green shading represents the regression coefficients for BHI, while hatching shows areas where ENSO is not significant in the model. In (c) the green shading represents the regression coefficients for ENSO, while hatching show areas where BHI is not significant in the model.

with TCP. This is not necessarily enough to illuminate how the relationship changes in the presence of competing climatic controls. To better understand the connection between TCP, NASH, and ENSO, we performed a linear regression analysis, where the BHI and ENSO–BEST were used as predictors (Fig. 8). Immediately, there are two distinct regions of significant R^2 values (Fig. 8a): a large swath of relatively high values that extends from the Gulf Coast to the northern Mid-Atlantic, and a smaller area in south-central Texas and northeast Florida. These areas correspond to the BHI and ENSO, respectively. Maps of the regression coefficients for BHI (Fig. 8b) and ENSO (Fig. 8c) show similar regionalization as the R^2 values (Fig. 8a). Interestingly, in areas where a significant relationship is seen between BHI (ENSO) and TCP, ENSO (BHI) is removed from the model, indicating that it exerts a limited influence on TCP (Figs. 8b,c). There are large areas where the influence of both BHI and ENSO is nonexistent (Figs. 8b,c), which is corroborated by the low R^2 values produced by the model (Fig. 8a). In either case, our regression model further supports our findings that the NASH, specifically the BHI, exhibits a greater influence on TCP variability in the study area.

We can further support these claims by examining TCP in the context of empirical orthogonal functions (EOFs). Eigenvector loading maps for total JJASON TCP indicate that the leading mode of variability, EOF 1, explains 17.9% of the total variance in the total seasonal TCP (Fig. 9). We also examined the eigenvectors of TCP contribution, which produced virtually identical loading maps (not shown). Similar to mean JJASON TCP and TCP contribution (Figs. 1 and 2), the highest loadings on EOF 1 occur in coastal North Carolina with slightly lower values occurring in southeast Louisiana and the central coastal plain (i.e., Alabama and Mississippi; Fig. 9). Beyond these locations, values are substantially lower (≤0.015) across the study region, with the exception of isolated areas of intermediate values (~0.025–0.030) along the coast. Distinct regionality is seen in EOFs 2–4, where the remaining EOFs explain 15.4% (EOF 2), 9.20% (EOF 3), and 6.50% (EOF 4) of the variability (Fig. 9). In EOF 2, the Northeast and coastal Texas have the opposite sign to much of the Southeast and Midwest. Additionally, the two extrema are located in North Carolina (≈−0.05) and Alabama (≥0.025). EOF 3 also shows a distinct dipole pattern throughout the study area. Finally, EOF 4 shows a more spatially heterogeneous pattern, with smaller regions of values of both signs.

Only the scores of EOF 1 had a significant correlation with BHI and ENSO. BHI showed a significant moderate correlation with the leading mode of variability ($r = 0.4327$; $p < 0.01$). Likewise, a significant relationship was observed between ENSO–BEST and EOF 1

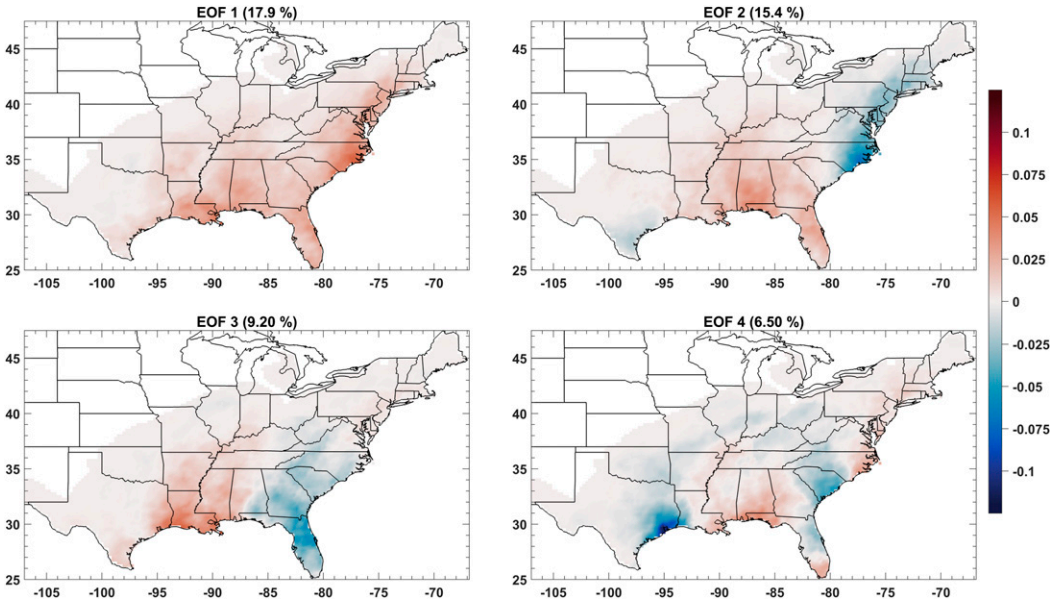

FIG. 9. Loading map of leading unrotated EOFs for mean JJASON TCP (mm) from 1948 to 2015. EOFs 1–4 account for 49% of the total variability.

($r = -0.2816$; $p < 0.05$). Our results suggest that both the NASH and ENSO are significantly connected to the distribution of seasonal TCP totals, with the former having a greater influence on TCP by way of controlling storm tracks.

The regionalization observed in the EOF analysis (Fig. 9) is corroborated by the grid-based correlation analysis between mean JJASON BHI/ENSO and total seasonal TCP (Figs. 6 and 7) and TCP contribution (not shown). Regions with the highest eigenvalues (Fig. 9; EOF 1) coincide with significant, weak to moderate positive correlations in similar locations in Louisiana and North Carolina (Figs. 6 and 7). The lowest eigenvalues (Fig. 9; EOF 1) coincide with weak to moderate negative correlations in similar locations in Texas (Figs. 6 and 7). Seasonal TCP totals (Fig. 6) and contributions (not shown) are positively correlated to BHI in southeast Louisiana and North Carolina, while a significant inverse relationship with ENSO is present in Texas (Fig. 7). Given that BHI and ENSO only have a significant relationship with TCP in Louisiana and North Carolina (Fig. 6) and Texas (Fig. 7), respectively, while also being distinct features in EOF 1 (Fig. 9), this could be indicative of a more nuanced relationship between TCP and large-scale circulation operating on regional scales or smaller. Unlike previous studies employing EOF analysis (e.g., Nogueira et al. 2013), our results suggest that the role of ENSO on TCP patterns is weaker and much more limited than BHI.

Nogueira et al. (2013) found a significant inverse correlation between ENSO and EOF 6, explaining 8% of the total variance. Our EOF analysis suggests that the role of ENSO on TCP patterns is more limited. While our use of a longer dataset could explain these differences, they are probably the result of dataset structure (i.e., gridded vs point; Ensor and Robeson 2008). Our linear regression model (Fig. 8) and EOF (Fig. 9) results both indicate that the NASH is a more important control on TCP patterns than ENSO, supporting our correlation analysis results (Figs. 6, 7). This is likely because the NASH acts as a blocking or steering mechanism for storm tracks (Vega and Binkley 1993; Elsner et al. 2000; Colbert and Soden 2012). However, variables such as North Atlantic SST patterns are also important controls on TCP variability (Rodgers et al. 1994; Villarini et al. 2014), and thus further examination of TCP controls is critical.

4. Conclusions

Precipitation from TCs is an integral component of regional hydroclimates in the eastern United States, where TCP can comprise a substantial percentage of total precipitation (Cry 1967; Knight and Davis 2007; Nogueira and Keim 2011). In this study we developed a high-resolution, gridded ($0.25° \times 0.25°$) dataset of TCP from 1948 to 2015 and examined TCP climatology in the eastern United States. The resulting spatial patterns generally corroborate previous studies (e.g., Knight and

Davis 2007; Nogueira and Keim 2011) with differences between studies likely resulting from the length and resolution/gridded nature of TCPDat and different TCP extraction criteria. Our results highlight the strengths and weaknesses of TCPDat. For example, the dataset provides a uniformly distributed grid of time series without missing values, which can be easily implemented into numerical models. TCPDat is based on URD, which does not represent individual extreme events well (Ensor and Robeson 2008). As such, this combined with the conservative search radius used in this study likely led to an underestimation of TCP. Nevertheless, this is generally not an issue when looking at TCP over seasonal, annual, or longer time scales (Ensor and Robeson 2008). Despite the fact that the gridded product underwent substantial interpolation, it still provides the most spatially consistent depiction of TCP. Finally, researchers can modify the search radius criteria to match their needs upon accessing the code via GitHub (https://github.com/jbregy/TCPDat.git).

We also used TCPDat to identify possible relationships between TCP patterns and large-scale atmospheric variability (ENSO and NASH). Our results suggest that spatiotemporal TCP variability is more closely linked to variability in the NASH and less so with ENSO. We found no studies examining a link between TCP and the NASH. However, given the influence of the NASH on TC tracks (e.g., Elsner et al. 2000) and hydroclimatic variability in the southeastern United States (Li et al. 2011, 2012), it is likely that variations in the position or strength of the NASH is a relatively important control on TCP variability. Even so, environmental (e.g., SSTs) and storm-specific variables likely exert a greater influence on TCP (Rodgers et al. 1994; Villarini et al. 2014; Hernández Ayala and Matyas 2016; Trenberth et al. 2018). As such, further examination of TCP controls is essential to elucidate the role of TCs in regional hydroclimates as well as how TCP will vary in a changing climate. Finally, TCPDat can be updated on an annual basis and serve as an important tool for continued research into the relationship between TCP and large-scale circulation. Understanding TCP variability can provide insight to additional areas including hazard mitigation (e.g., landslides, floods), risk assessment for insurance, or conservation/biodiversity practices. Fully understanding TCP variability requires thorough exploration of different TCP datasets, and is critical when preparing vulnerable communities for a changing climate.

Acknowledgments. We thank the three anonymous reviewers for providing constructive comments in order to vastly improve this paper. This project was partially funded by the National Science Foundation Grant NSF1660432.

REFERENCES

Antinao, J. L., and L. M. Farfán, 2013: Occurrence of landslides during the approach of tropical cyclone Juliette (2001) to Baja California Sur, Mexico. *Atmósfera*, **26**, 183–208, https://doi.org/10.1016/S0187-6236(13)71071-3.

Archambault, H. M., L. F. Bosart, D. Keyser, and A. R. Aiyyer, 2008: Influence of large-scale flow regimes on cool-season precipitation in the northeastern United States. *Mon. Wea. Rev.*, **136**, 2945–2963, https://doi.org/10.1175/2007MWR2308.1.

Aryal, Y. N., G. Villarini, W. Zhang, and G. A. Vecchi, 2018: Long term changes in flooding and heavy rainfall associated with North Atlantic tropical cyclones: Roles of the North Atlantic Oscillation and El Niño–Southern Oscillation. *J. Hydrol.*, **559**, 698–710, https://doi.org/10.1016/j.jhydrol.2018.02.072.

Ashouri, H., K. L. Hsu, S. Sorooshian, D. K. Braithwaite, K. R. Knapp, L. D. Cecil, B. R. Nelson, and O. P. Prat, 2015: PERSIANN-CDR: Daily precipitation climate data record from multisatellite observations for hydrological and climate studies. *Bull. Amer. Meteor. Soc.*, **96**, 69–83, https://doi.org/10.1175/BAMS-D-13-00068.1.

Atallah, E., L. F. Bosart, and A. R. Aiyyer, 2007: Precipitation distribution associated with landfalling tropical cyclones over the eastern United States. *Mon. Wea. Rev.*, **135**, 2185–2206, https://doi.org/10.1175/MWR3382.1.

Benedetti, A., P. Lopez, E. Moreau, P. Bauer, and V. Venugopal, 2005: Verification of TMI-adjusted rainfall analyses of tropical cyclones at ECMWF using TRMM precipitation radar. *J. Appl. Meteor.*, **44**, 1677–1690, https://doi.org/10.1175/JAM2300.1.

Bove, M. C., J. B. Elsner, C. W. Landsea, X. Niu, and J. J. O'Brien, 1998: Effect of El Niño on U.S. landfalling hurricanes, revisited. *Bull. Amer. Meteor. Soc.*, **79**, 2477–2482, https://doi.org/10.1175/1520-0477(1998)079<2477:EOENOO>2.0.CO;2.

Brun, J., and A. P. Barros, 2014: Mapping the role of tropical cyclones on the hydroclimate of the southeast United States: 2002–2011. *Int. J. Climatol.*, **34**, 494–517, https://doi.org/10.1002/joc.3703.

Chen, M., W. Shi, P. Xie, V. B. S. Silva, V. E. Kousky, R. Wayne Higgins, and J. E. Janowiak, 2008: Assessing objective techniques for gauge-based analyses of global daily precipitation. *J. Geophys. Res.*, **113**, D04110, https://doi.org/10.1029/2007JD009132.

Chi, C.-H., R. W. McEwan, C.-T. Chang, C. Zheng, Z. Yang, J.-M. Chiang, and T.-C. Lin, 2015: Typhoon disturbance mediates elevational patterns of forest structure, but not species diversity, in humid monsoon Asia. *Ecosystems*, **18**, 1410–1423, https://doi.org/10.1007/s10021-015-9908-3.

Chien, F. C., and H. C. Kuo, 2011: On the extreme rainfall of Typhoon Morakot (2009). *J. Geophys. Res.*, **116**, D05104, https://doi.org/10.1029/2010JD015092.

Cogan, J., I. Gratchev, and G. Wang, 2018: Rainfall-induced shallow landslides caused by ex-Tropical Cyclone Debbie, 31st March 2017. *Landslides*, **15**, 1215–1221, https://doi.org/10.1007/s10346-018-0982-4.

Colbert, A. J., and B. J. Soden, 2012: Climatological variations in North Atlantic tropical cyclone tracks. *J. Climate*, **25**, 657–673, https://doi.org/10.1175/JCLI-D-11-00034.1.

Corbosiero, K. L., M. J. Dickinson, and L. F. Bosart, 2009: The contribution of eastern North Pacific tropical cyclones to the rainfall climatology of the southwest United States. *Mon. Wea. Rev.*, **137**, 2415–2435, https://doi.org/10.1175/2009MWR2768.1.

Cressman, G. P., 1959: An operational objective analysis system. *Mon. Wea. Rev.*, **87**, 367–374, https://doi.org/10.1175/1520-0493(1959)087<0367:AOOAS>2.0.CO;2.

Cry, G. W., 1967: Effects of tropical cyclone rainfall on the distribution of precipitation over the eastern and southern United States. United States Environmental Science Services Administration, ESSA Professional Papers, Vol. 1, 67 pp.

Czajkowski, J., G. Villarini, E. Michel-Kerjan, and J. A. Smith, 2013: Determining tropical cyclone inland flooding loss on a large scale through a new flood peak ratio-based methodology. *Environ. Res. Lett.*, **8**, 044056, https://doi.org/10.1088/1748-9326/8/4/044056.

Davis, R. E., B. P. Hayden, D. Gay, W. L. Phillips, and G. V. Jones, 1997: The North Atlantic subtropical anticyclone. *J. Climate*, **10**, 728–744, https://doi.org/10.1175/1520-0442(1997)010<0728:TNASA>2.0.CO;2.

Deng, Z., and Coauthors, 2015: Impacts of tropical cyclones and accompanying precipitation on infectious diarrhea in cyclone landing areas of Zhejiang Province, China. *Int. J. Environ. Res. Public Health*, **12**, 1054–1068, https://doi.org/10.3390/ijerph120201054.

Elsner, J. B., and B. Kocher, 2000: Global tropical cyclone activity: A link to the North Atlantic Oscillation. *Geophys. Res. Lett.*, **27**, 129–132, https://doi.org/10.1029/1999GL010893.

——, K. Liu, and B. Kocher, 2000: Spatial variations in major U.S. hurricane activity: Statistics and a physical mechanism. *J. Climate*, **13**, 2293–2305, https://doi.org/10.1175/1520-0442(2000)013<2293:SVIMUS>2.0.CO;2.

——, B. H. Bossak, and X. F. Niu, 2001: Secular changes to the ENSO–U.S. hurricane relationship. *Geophys. Res. Lett.*, **28**, 4123–4126, https://doi.org/10.1029/2001GL013669.

Enfield, D. B., and L. Cid-Serrano, 2010: Secular and multidecadal warmings in the North Atlantic and their relationships with major hurricane activity. *Int. J. Climatol.*, **30**, 174–184, https://doi.org/10.1002/JOC.1881.

Ensor, L. A., and S. M. Robeson, 2008: Statistical characteristics of daily precipitation: Comparisons of gridded and point datasets. *J. Appl. Meteor. Climatol.*, **47**, 2468–2476, https://doi.org/10.1175/2008JAMC1757.1.

Evans, J. L., and R. E. Hart, 2003: Objective indicators of the life cycle evolution of extratropical transition for Atlantic tropical cyclones. *Mon. Wea. Rev.*, **131**, 909–925, https://doi.org/10.1175/1520-0493(2003)131<0909:OIOTLC>2.0.CO;2.

Ficklin, D. L., J. T. Maxwell, S. L. Letsinger, and H. Gholizadeh, 2015: A climatic deconstruction of recent drought trends in the United States. *Environ. Res. Lett.*, **10**, 044009, https://doi.org/10.1088/1748-9326/10/4/044009.

Fredrick, T., M. Ponnaiah, M. V. Murhekar, Y. Jayaraman, J. K. David, S. Vadivoo, and V. Joshua, 2015: Cholera outbreak linked with lack of safe water supply following a tropical cyclone in Pondicherry, India, 2012. *J. Health Popul. Nutr.*, **33**, 31–38, https://www.ncbi.nlm.nih.gov/pubmed/25995719.

Gandin, L. S., 1965: *Objective Analysis of Meteorological Fields*. Israel Program for Scientific Translations, 242 pp.

Glaser, P. H., B. C. S. Hansen, J. J. Donovan, T. J. Givnish, C. A. Stricker, and J. C. Volin, 2013: Holocene dynamics of the Florida Everglades with respect to climate, dustfall, and tropical storms. *Proc. Natl. Acad. Sci. USA*, **110**, 17 211–17 216, https://doi.org/10.1073/pnas.1222239110.

Gocic, M., and S. Trajkovic, 2013: Analysis of changes in meteorological variables using Mann-Kendall and Sen's slope estimator statistical tests in Serbia. *Global Planet. Change*, **100**, 172–182, https://doi.org/10.1016/j.gloplacha.2012.10.014.

Goulding, W., P. T. Moss, and C. A. McAlpine, 2016: Cascading effects of cyclones on the biodiversity of southwest Pacific islands. *Biol. Conserv.*, **193**, 143–152, https://doi.org/10.1016/j.biocon.2015.11.022.

Gray, W. M., 1984: Atlantic seasonal hurricane frequency. Part I: El Niño and 30 mb quasi-biennial oscillation influences. *Mon. Wea. Rev.*, **112**, 1649–1668, https://doi.org/10.1175/1520-0493(1984)112<1649:ASHFPI>2.0.CO;2.

Guiney, J., 2007: How county/city emergency managers can assess vulnerability to hurricanes, develop response plans and mitigate risk. *J. Bus. Continuity Emerg. Plann.*, **2**, 92–109.

Hagen, A. B., D. Strahan-Sakoskie, and C. Luckett, 2012: A reanalysis of the 1944–53 Atlantic hurricane seasons—The first decade of aircraft reconnaissance. *J. Climate*, **25**, 4441–4460, https://doi.org/10.1175/JCLI-D-11-00419.1.

Hall, J. D., M. Xue, L. Ran, and L. M. Leslie, 2013: High-resolution modeling of Typhoon Morakot (2009): Vortex Rossby waves and their role in extreme precipitation over Taiwan. *J. Atmos. Sci.*, **70**, 163–186, https://doi.org/10.1175/JAS-D-11-0338.1.

Hart, R. E., and J. L. Evans, 2001: A climatology of the extratropical transition of Atlantic tropical cyclones. *J. Climate*, **14**, 546–564, https://doi.org/10.1175/1520-0442(2001)014<0546:ACOTET>2.0.CO;2.

——, ——, and C. Evans, 2006: Synoptic composites of the extratropical transition life cycle of North Atlantic tropical cyclones: Factors determining posttransition evolution. *Mon. Wea. Rev.*, **134**, 553–578, https://doi.org/10.1175/MWR3082.1.

Harville, S., 2009: Effects of Appalachian topography on precipitation from landfalling hurricanes. North Carolina State University, 315 pp.

Hernández Ayala, J. J., and C. J. Matyas, 2016: Tropical cyclone rainfall over Puerto Rico and its relations to environmental and storm-specific factors. *Int. J. Climatol.*, **36**, 2223–2237, https://doi.org/10.1002/joc.4490.

Hewitson, B. C., and R. G. Crane, 2005: Gridded area-averaged daily precipitation via conditional interpolation. *J. Climate*, **18**, 41–57, https://doi.org/10.1175/JCLI3246.1.

Higgins, R. W., and V. E. Kousky, 2013: Changes in observed daily precipitation over the United States between 1950–79 and 1980–2009. *J. Hydrometeor.*, **14**, 105–121, https://doi.org/10.1175/JHM-D-12-062.1.

——, E. Yarosh, and W. Shi, 2000a: CPC Unified Gauge-Based Analysis of Daily Precipitation over CONUS. NCEP/CPC and ESRL/Physical Sciences Division, accessed 14 March 2017, https://www.esrl.noaa.gov/psd/data/gridded/data.unified.daily.conus.html.

——, W. Shi, E. Yarosh, and R. Joyce, 2000b: Improved United States Precipitation Quality Control System and Analysis. Climate Prediction Center Atlas No. 7, accessed 14 March 2017, https://www.cpc.ncep.noaa.gov/research_papers/ncep_cpc_atlas/7/.

——, V. B. S. Silva, W. Shi, and J. Larson, 2007: Relationships between climate variability and fluctuations in daily precipitation over the United States. *J. Climate*, **20**, 3561–3579, https://doi.org/10.1175/JCLI4196.1.

——, ——, V. E. Kousky, and W. Shi, 2008: Comparison of daily precipitation statistics for the United States in observations and in the NCEP Climate Forecast System. *J. Climate*, **21**, 5993–6014, https://doi.org/10.1175/2008JCLI2339.1.

Jiang, H., and E. J. Zipser, 2010: Contribution of tropical cyclones to the global precipitation from eight seasons of TRMM data: Regional, seasonal, and interannual variations. *J. Climate*, **23**, 1526–1543, https://doi.org/10.1175/2009JCLI3303.1.

——, and E. M. Ramirez, 2013: Necessary conditions for tropical cyclone rapid intensification as derived from 11 years of TRMM data. *J. Climate*, **26**, 6459–6470, https://doi.org/10.1175/JCLI-D-12-00432.1.

Kam, J., J. Sheffield, and E. F. Wood, 2014: A multiscale analysis of drought and pluvial mechanisms for the southeastern United

States. *J. Geophys. Res.*, **119**, 7348–7367, https://doi.org/10.1002/2014JD021453.

Katz, R. W., M. B. Parlange, and C. Tebaldi, 2003: Stochastic modeling of the effects of large-scale circulation on daily weather in the southeastern U.S. *Climatic Change*, **60**, 189–216, https://doi.org/10.1023/A:1026054330406.

Khouakhi, A., G. Villarini, and G. A. Vecchi, 2017: Contribution of tropical cyclones to rainfall at the global scale. *J. Climate*, **30**, 359–372, https://doi.org/10.1175/JCLI-D-16-0298.1.

Kim, S., Y. Shin, H. Kim, H. Pak, and J. Ha, 2013: Impacts of typhoon and heavy rain disasters on mortality and infectious diarrhea hospitalization in South Korea. *Int. J. Environ. Health Res.*, **23**, 365–376, https://doi.org/10.1080/09603123.2012.733940.

Klotzbach, P. J., and W. M. Gray, 2008: Multidecadal variability in North Atlantic tropical cyclone activity. *J. Climate*, **21**, 3929–3935, https://doi.org/10.1175/2008JCLI2162.1.

Knapp, K. R., M. C. Kruk, D. H. Levinson, H. J. Diamond, and C. Neumann, 2010: The International Best Track Archive for Climate Stewardship (IBTrACS) project: Unifying tropical cyclone data. *Bull. Amer. Meteor. Soc.*, **91**, 363–376, https://doi.org/10.1175/2009BAMS2755.1.

Knapp, P. A., J. T. Maxwell, and P. T. Soulé, 2016: Tropical cyclone rainfall variability in coastal North Carolina derived from longleaf pine (*Pinus palustris* Mill.): AD 1771–2014. *Climatic Change*, https://doi.org/10.1007/s10584-015-1560-6.

Knight, D. B., and R. E. Davis, 2007: Climatology of tropical cyclone rainfall in the southeastern United States. *Phys. Geogr.*, **28**, 126–147, https://doi.org/10.2747/0272-3646.28.2.126.

——, and ——, 2009: Contribution of tropical cyclones to extreme rainfall events in the southeastern United States. *J. Geophys. Res.*, **114**, D23102, https://doi.org/10.1029/2009JD012511.

Konrad, C. E., and L. B. Perry, 2010: Relationships between tropical cyclones and heavy rainfall in the Carolina region of the USA. *Int. J. Climatol.*, **30**, 522–534, https://doi.org/10.1002/JOC.1894.

——, M. F. Meaux, and D. A. Meaux, 2002: Relationships between tropical cyclone attributes and precipitation totals: Considerations of scale. *Int. J. Climatol.*, **22**, 237–247, https://doi.org/10.1002/joc.721.

Kuo, Y. S., Y. J. Tsai, Y. S. Chen, C. L. Shieh, K. Miyamoto, and T. Itoh, 2013: Movement of deep-seated rainfall-induced landslide at Hsiaolin Village during Typhoon Morakot. *Landslides*, **10**, 191–202, https://doi.org/10.1007/s10346-012-0315-y.

Landsea, C. W., and J. L. Franklin, 2013: Atlantic hurricane database uncertainty and presentation of a new database format. *Mon. Wea. Rev.*, **141**, 3576–3592, https://doi.org/10.1175/MWR-D-12-00254.1.

——, and Coauthors, 2004: The Atlantic Hurricane Database Re-Analysis Project: Documentation for 1851–1910 alterations and additions to the HURDAT database. *Hurricanes and Typhoons: Past, Present, and Future*, R. J. Murnane and K. Liu, Eds., Columbia University Press, 178–221.

——, A. Hagen, W. Bredemeyer, C. Carrasco, D. A. Glenn, A. Santiago, D. Strahan-Sakoskie, and M. Dickinson, 2014: A reanalysis of the 1931–43 Atlantic hurricane database. *J. Climate*, **27**, 6093–6118, https://doi.org/10.1175/JCLI-D-13-00503.1.

Li, J., and J. X. L. Wang, 2003: A new North Atlantic oscillation index and its variability. *Adv. Atmos. Sci.*, **20**, 661–676, https://doi.org/10.1007/BF02915394.

Li, L., W. Li, and Y. Kushnir, 2012: Variation of the North Atlantic subtropical high western ridge and its implication to southeastern US summer precipitation. *Climate Dyn.*, **39**, 1401–1412, https://doi.org/10.1007/s00382-011-1214-y.

Li, W., L. Li, R. Fu, Y. Deng, and H. Wang, 2011: Changes to the North Atlantic subtropical high and its role in the intensification of summer rainfall variability in the southeastern United States. *J. Climate*, **24**, 1499–1506, https://doi.org/10.1175/2010JCLI3829.1.

Lin, C. Y., N. C. Chiu, and C. M. Lee, 2012: Leptospirosis after typhoon. *Amer. J. Trop. Med. Hyg.*, **86**, 187–188, https://doi.org/10.4269/ajtmh.2012.11-0518.

Lin, G.-W., H. Chen, N. Hovius, M.-J. Horng, S. Dadson, P. Meunier, and M. Lines, 2008: Effects of earthquake and cyclone sequencing on landsliding and fluvial sediment transfer in a mountain catchment. *Earth Surf. Processes Landforms*, **33**, 1354–1373, https://doi.org/10.1002/esp.1716.

Liu, K., and M. L. Fearn, 2000: Reconstruction of prehistoric landfall frequencies of catastrophic hurricanes in northwestern Florida from lake sediment records. *Quat. Res.*, **54**, 238–245, https://doi.org/10.1006/qres.2000.2166.

Liu, L., Y.-L. Lin, and S.-H. Chen, 2016: Effects of landfall location and approach angle of an idealized tropical cyclone over a long mountain range. *Front. Earth Sci.*, **4**, 14, https://doi.org/10.3389/feart.2016.00014.

Lonfat, M., F. D. Marks, and S. S. Chen, 2004: Precipitation distribution in tropical cyclones using the Tropical Rainfall Measuring Mission (TRMM) microwave imager: A global perspective. *Mon. Wea. Rev.*, **132**, 1645–1660, https://doi.org/10.1175/1520-0493(2004)132<1645:PDITCU>2.0.CO;2.

Luitel, B., G. Villarini, and G. A. Vecchi, 2018: Verification of the skill of numerical weather prediction models in forecasting rainfall from U.S. landfalling tropical cyclones. *J. Hydrol.*, **556**, 1026–1037, https://doi.org/10.1016/j.jhydrol.2016.09.019.

Matyas, C. J., 2007: Quantifying the shapes of U.S. landfalling tropical cyclone rain shields. *Prof. Geogr.*, **59**, 158–172, https://doi.org/10.1111/j.1467-9272.2007.00604.x.

——, 2010: Associations between the size of hurricane rain fields at landfall and their surrounding environments. *Meteor. Atmos. Phys.*, **106**, 135–148, https://doi.org/10.1007/s00703-009-0056-1.

——, 2013: Processes influencing rain-field growth and decay after tropical cyclone landfall in the United States. *J. Appl. Meteor. Climatol.*, **52**, 1085–1096, https://doi.org/10.1175/JAMC-D-12-0153.1.

——, 2017: Comparing the spatial patterns of rainfall and atmospheric moisture among tropical cyclones having a track similar to Hurricane Irene (2011). *Atmosphere*, **8**, 165, https://doi.org/10.3390/ATMOS8090165.

Maxwell, J. T., P. T. Soulé, J. T. Ortegren, and P. A. Knapp, 2012: Drought-busting tropical cyclones in the southeastern Atlantic United States: 1950–2008. *Ann. Assoc. Amer. Geogr.*, **102**, 259–275, https://doi.org/10.1080/00045608.2011.596377.

——, J. T. Ortegren, P. A. Knapp, and P. T. Soulé, 2013: Tropical cyclones and drought amelioration in the Gulf and southeastern coastal United States. *J. Climate*, **26**, 8440–8452, https://doi.org/10.1175/JCLI-D-12-00824.1.

——, P. A. Knapp, J. T. Ortegren, D. L. Ficklin, and P. T. Soulé, 2017: Changes in the mechanisms causing rapid drought cessation in the southeastern United States. *Geophys. Res. Lett.*, **44**, 12 476–12 483, https://doi.org/10.1002/2017GL076261.

McCloskey, T. A., T. A. Bianchette, and K.-B. Liu, 2013: Track patterns of landfalling and coastal tropical cyclones in the Atlantic Basin, their relationship with the North Atlantic Oscillation (NAO), and the potential effect of global warming.

Amer. J. Climate Change, **2**, 12–22, https://doi.org/10.4236/ajcc.2013.23A002.

Mondoro, A., and D. M. Frangopol, 2018: Risk-based cost-benefit analysis for the retrofit of bridges exposed to extreme hydrologic events considering multiple failure modes. *Eng. Struct.*, **159**, 310–319, https://doi.org/10.1016/j.engstruct.2017.12.029.

Nogueira, R. C., and B. D. Keim, 2010: Annual volume and area variations in tropical cyclone rainfall over the eastern United States. *J. Climate*, **23**, 4363–4374, https://doi.org/10.1175/2010JCLI3443.1.

——, and ——, 2011: Contributions of Atlantic tropical cyclones to monthly and seasonal rainfall in the eastern United States 1960–2007. *Theor. Appl. Climatol.*, **103**, 213–227, https://doi.org/10.1007/s00704-010-0292-9.

——, ——, D. P. Brown, and K. D. Robbins, 2013: Variability of rainfall from tropical cyclones in the eastern USA and its association to the AMO and ENSO. *Theor. Appl. Climatol.*, **112**, 273–283, https://doi.org/10.1007/s00704-012-0722-y.

Ortegren, J. T., and J. T. Maxwell, 2014: Spatiotemporal patterns of drought/tropical cyclone co-occurrence in the Southeastern USA: Linkages to North Atlantic climate variability. *Geogr. Compass*, **8**, 540–559, https://doi.org/10.1111/gec3.12148.

——, P. A. Knapp, J. T. Maxwell, W. P. Tyminski, and P. T. Soulé, 2011: Ocean–atmosphere influences on low-frequency warm-season drought variability in the Gulf Coast and southeastern United States. *J. Appl. Meteor. Climatol.*, **50**, 1177–1186, https://doi.org/10.1175/2010JAMC2566.1.

Prat, O. P., and B. R. Nelson, 2013a: Precipitation contribution of tropical cyclones in the southeastern United States from 1998 to 2009 using TRMM satellite data. *J. Climate*, **26**, 1047–1062, https://doi.org/10.1175/JCLI-D-11-00736.1.

——, and ——, 2013b: Mapping the world's tropical cyclone rainfall contribution over land using the TRMM multi-satellite precipitation analysis. *Water Resour. Res.*, **49**, 7236–7254, https://doi.org/10.1002/wrcr.20527.

Rios Gaona, M. F., G. Villarini, W. Zhang, and G. A. Vecchi, 2018: The added value of IMERG in characterizing rainfall in tropical cyclones. *Atmos. Res.*, **209**, 95–102, https://doi.org/10.1016/j.atmosres.2018.03.008.

Risser, M. D., and M. F. Wehner, 2017: Attributable human-induced changes in the likelihood and magnitude of the observed extreme precipitation during Hurricane Harvey. *Geophys. Res. Lett.*, **44**, 12 457–12 464, https://doi.org/10.1002/2017GL075888.

Rodgers, E. B., and H. F. Pierce, 1995: A satellite observation study of precipitation characteristics in western North Pacific tropical cyclones. *J. Appl. Meteor. Climatol.*, **34**, 2587–2599, https://doi.org/10.1175/1520-0450(1995)034<2587:ASOSOP>2.0.CO;2.

——, S. W. Chang, and H. F. Pierce, 1994: A satellite observational and numerical study of precipitation characteristics in western North Atlantic tropical cyclones. *J. Appl. Meteor. Climatol.*, **33**, 129–139, https://doi.org/10.1175/1520-0450(1994)033<0129:ASOANS>2.0.CO;2.

——, R. F. Adler, and H. F. Pierce, 2001: Contribution of tropical cyclones to the North Atlantic climatological rainfall as observed from satellites. *J. Appl. Meteor. Climatol.*, **40**, 1785–1800, https://doi.org/10.1175/1520-0450(2001)040<1785:COTCTT>2.0.CO;2.

Rostom, R., and Y.-L. Lin, 2015: Control parameters for track continuity of cyclones passing over the south-central Appalachian Mountains. *Wea. Forecasting*, **30**, 1429–1449, https://doi.org/10.1175/WAF-D-14-00080.1.

Sahsamanoglou, H. S., 1990: A contribution to the study of action centres in the North Atlantic. *Int. J. Climatol.*, **10**, 247–261, https://doi.org/10.1002/joc.3370100303.

Schwarz, F. K., 1970: The unprecedented rains in Virginia associated with the remnants of Hurricane Camille. *Mon. Wea. Rev.*, **98**, 851–859, https://doi.org/10.1175/1520-0493(1970)098<0851:TURIVA>2.3.CO;2.

Shepard, D., 1968: A two-dimensional interpolation function for irregularly-spaced data. *Proceedings of the 1968 23rd ACM National Conference*, ACM Press, 517–524, http://portal.acm.org/citation.cfm?doid=800186.810616.

Shepherd, J. M., A. Grundstein, and T. L. Mote, 2007: Quantifying the contribution of tropical cyclones to extreme rainfall along the coastal southeastern United States. *Geophys. Res. Lett.*, **34**, L23810, https://doi.org/10.1029/2007GL031694.

Smith, C. A., and P. Sardeshmukh, 2000: The effect of ENSO on the intraseasonal variance of surface temperature in winter. *Int. J. Climatol.*, **20**, 1543–1557, https://doi.org/10.1002/1097-0088(20001115)20:13<1543::AID-JOC579>3.0.CO;2-A.

Smith, S. R., J. Brolley, J. J. O'Brien, and C. A. Tartaglione, 2007: ENSO's impact on regional U.S. hurricane activity. *J. Climate*, **20**, 1404–1414, https://doi.org/10.1175/JCLI4063.1.

Stahle, D. W., and M. K. Cleaveland, 1992: Reconstruction and analysis of spring rainfall over the southeastern U.S. for the past 1000 years. *Bull. Amer. Meteor. Soc.*, **73**, 1947–1961, https://doi.org/10.1175/1520-0477(1992)073<1947:RAAOSR>2.0.CO;2.

Tabari, H., B. S. Somee, and M. R. Zadeh, 2011: Testing for long-term trends in climatic variables in Iran. *Atmos. Res.*, **100**, 132–140, https://doi.org/10.1016/j.atmosres.2011.01.005.

Tang, J., and C. J. Matyas, 2018: A nowcasting model for tropical cyclone precipitation regions based on the TREC motion vector retrieval with a semi-Lagrangian scheme for Doppler weather radar. *Atmosphere*, **9**, 200, https://doi.org/10.3390/atmos9050200.

Thyng, K. M., C. A. Greene, R. D. Hetland, H. M. Zimmerle, and S. F. DiMarco, 2016: True colors of oceanography: Guidelines for effective and accurate colormap selection. *Oceanography*, **29**, 9–13, https://doi.org/10.5670/oceanog.2016.66.

Torn, R. D., and C. Snyder, 2012: Uncertainty of tropical cyclone best-track information. *Wea. Forecasting*, **27**, 715–729, https://doi.org/10.1175/WAF-D-11-00085.1.

Trenberth, K. E., L. Cheng, P. Jacobs, Y. Zhang, and J. Fasullo, 2018: Hurricane Harvey links to ocean heat content and climate change adaptation. *Earth's Future*, **6**, 730–744, https://doi.org/10.1029/2018EF000825.

Vecchi, G. A., and T. R. Knutson, 2011: Estimating annual numbers of Atlantic hurricanes missing from the HURDAT database (1878–1965) using ship track density. *J. Climate*, **24**, 1736–1746, https://doi.org/10.1175/2010JCLI3810.1.

Vega, A. J., and M. S. Binkley, 1993: Tropical cyclone formation in the North Atlantic Basin, 1960–1989. *Climate Res.*, **3**, 221–232, https://doi.org/10.3354/cr003221.

Villarini, G., J. A. Smith, M. L. Baeck, T. Marchok, and G. A. Vecchi, 2011: Characterization of rainfall distribution and flooding associated with U.S. landfalling tropical cyclones: Analyses of Hurricanes Frances, Ivan, and Jeanne (2004). *J. Geophys. Res.*, **116**, D23116, https://doi.org/10.1029/2011JD016175.

——, D. A. Lavers, E. Scoccimarro, M. Zhao, M. F. Wehner, G. A. Vecchi, T. R. Knutson, and K. A. Reed, 2014: Sensitivity of tropical cyclone rainfall to idealized global-scale forcings. *J. Climate*, **27**, 4622–4641, https://doi.org/10.1175/JCLI-D-13-00780.1.

Walls, S., W. Barichivich, and M. Brown, 2013: Drought, deluge and declines: The impact of precipitation extremes on amphibians in a changing climate. *Biology*, **2**, 399–418, https://doi.org/10.3390/BIOLOGY2010399.

Wang, C., S. K. Lee, and D. B. Enfield, 2008: Atlantic warm pool acting as a link between Atlantic Multidecadal Oscillation and Atlantic tropical cyclone activity. *Geochem. Geophys. Geosyst.*, **9**, Q05V03, https://doi.org/10.1029/2007GC001809.

Wooten, R. M., K. A. Gillon, A. C. Witt, R. S. Latham, T. J. Douglas, J. B. Bauer, S. J. Fuemmeler, and L. G. Lee, 2008: Geologic, geomorphic, and meteorological aspects of debris flows triggered by Hurricanes Frances and Ivan during September 2004 in the southern Appalachian Mountains of Macon County, North Carolina (southeastern USA). *Landslides*, **5**, 31–44, https://doi.org/10.1007/s10346-007-0109-9.

Xie, P., M. Chen, S. Yang, A. Yatagai, T. Hayasaka, Y. Fukushima, and C. Liu, 2007: A gauge-based analysis of daily precipitation over East Asia. *J. Hydrometeor.*, **8**, 607–626, https://doi.org/10.1175/JHM583.1.

Xu, W., H. Jiang, and X. Kang, 2014: Rainfall asymmetries of tropical cyclones prior to, during, and after making landfall in south China and southeast United States. *Atmos. Res.*, **139**, 18–26, https://doi.org/10.1016/j.atmosres.2013.12.015.

Yang, K., and Coauthors, 2019: Incorporating inland flooding into hurricane evacuation decision support modeling. *Nat. Hazards*, **96**, 857–878, https://doi.org/10.1007/S11069-019-03573-9.

Yang, R., A. Fairley, and W. Park, 2018: The centennial variation of El Niño impact on Atlantic tropical cyclones. *Earth Interact.*, **22**, 1–15, https://doi.org/10.1175/EI-D-17-0006.1.

Yanites, B. J., and Coauthors, 2018: Landslides control the spatial and temporal variations of channel width in southern Taiwan: implications for landscape evolution and cascading hazards in steep, tectonically active landscapes. *Earth Surf. Processes Landforms*, **43**, 1782–1797, https://doi.org/10.1002/esp.4353.

Zhang, W., G. Villarini, G. A. Vecchi, and J. A. Smith, 2018: Urbanization exacerbated the rainfall and flooding caused by hurricane Harvey in Houston. *Nature*, **563**, 384–388, https://doi.org/10.1038/s41586-018-0676-z.

Zheng, J., W. Han, B. Jiang, W. Ma, and Y. Zhang, 2017: Infectious diseases and tropical cyclones in southeast China. *Int. J. Environ. Res. Public Health*, **14**, 494, https://doi.org/10.3390/ijerph14050494.

Zhou, Y., and C. J. Matyas, 2017: Spatial characteristics of storm-total rainfall swaths associated with tropical cyclones over the eastern United States. *Int. J. Climatol.*, **37**, 557–569, https://doi.org/10.1002/joc.5021.

Zhu, L., and S. M. Quiring, 2017: An extraction method for long-term tropical cyclone precipitation from daily rain gauges. *J. Hydrometeor.*, **18**, 2559–2576, https://doi.org/10.1175/JHM-D-16-0291.1.

Zhu, T., and D.-L. Zhang, 2006: Numerical simulation of Hurricane Bonnie (1998). Part II: sensitivity to varying cloud microphysical processes. *J. Atmos. Sci.*, **63**, 109–126, https://doi.org/10.1175/JAS3599.1.

Zick, S. E., and C. J. Matyas, 2015: Tropical cyclones in the North American Regional Reanalysis: An assessment of spatial biases in location, intensity, and structure. *J. Geophys. Res.*, **120**, 1651–1669, https://doi.org/10.1002/2014JD022417.